Article

Linearly Swept Tunable Laser Source with Closed-Loop Control of Drive Waveform

Yunhae Yeh

College of Electronics and Information, Kyung Hee University, Yongin 17104, Korea; yhyh@khu.ac.kr

Abstract: A method for a linearly swept tunable laser source with a simple configuration is proposed. The principle of the method is based on the fact that the interval of the transmission peaks of a fixed etalon can be used as a stable reference. The reference provided by the fixed etalon is used to deform the drive signal waveform for linear optical-frequency tuning. To verify the validity of the methodology, an optical system augmented with two fiber Bragg gratings, one fixed etalon, and a dedicated signal-processing circuit was built and experimentally tested, confirming that it works well for a linearly tuned tunable laser source. Moreover, the potential for extending the scope of the application of the proposed method is suggested and some ways to improve its performance are also discussed.

Keywords: tunable laser; linear frequency tuning; tunable filter

Publisher's Note: MDPI stays neutral with regard to jurisdictional claims in published maps and institutional affiliations.

1. Introduction

One of the most important elements in the field of optical-frequency domain reflectometry (OFDR) and fiber Bragg grating (FBG) sensor applications is a tunable laser source (TLS) [1–3]. A TLS with linear tuning over a wide range, which is required to avoid degradations in spatial resolutions and limitations in measurement lengths of the OFDR sensing system [4], is especially desirable. Linearly tuned TLSs have been implemented using external cavities, microwave modulators, electronic means, optical means, and other methods [5–7]. Although each method meets the required performance level in a specific application, a suitable method for implementing stable low-cost high-speed linearly tuned TLSs with wide tuning ranges and simple configurations has not yet been reported. In particular, a linearly tuned TLS with a wide range has not been easy to implement. As a result, non-linearly tuned TLSs with wide ranges have been used for OFDR systems, and performance limitations due to non-linearity have had to be addressed using an auxiliary interferometer to generate trigger clocks for use in data acquisition to compensate for tuning errors [1].

Piezoelectric transducers (PZTs), which contract or expand in response to accumulated electric charges, have been widely used in many applications. However, they are difficult devices to use because they are very sensitive to environmental variables and exhibit many intractable characteristics, such as non-linearity and hysteresis. A PZT can be modeled as a capacitor, so when a DC current flows in, the voltage across the capacitor increases linearly with time and the PZT expands almost linearly. Since a PZT does not have moving parts and can operate stably at a high speed, a PZT-actuated tunable filter (PZT-TF) can be tuned at a high speed over a wide wavelength range. Therefore, a configuration with a PZT-TF is considered a good choice for implementing a TLS operating at a high speed over a wide tuning range. A TLS adopting a PZT-TF can operate at a high speed, and its tuning range is wide, indicating that it has the potential to be a proper choice for the applications listed above if it is built for linear tuning [8].

In order to implement a linearly tuned TLS that is free from the influence of the non-idealities of PZT, such as non-linearity, hysteresis, creep, and environmental changes, a

device capable of monitoring the frequency change of a light source is required. Candidates for frequency monitoring devices, which can supply wavelength references, include microwave modulators [5], gas cells [9], FBGs [10], fixed etalons [11], and diffraction gratings, as mentioned above. The devices chosen in this study were a fixed etalon and an FBG. Fixed etalons generate transmission peaks at constant frequency intervals of $\Delta \nu = c/2nt$, where t is the thickness of the etalon and n is the refractive index of the etalon. With a 1 mm thick fused-silica etalon, a series of peaks of 100 GHz spacing can be obtained. Thus, we can have 100 reference peaks over a tuning range of 80 nm at 1550 nm. Fused silica is pretty insensitive to changes in its surrounding environment, so the peak spacing can be used as a very stable reference.

An FBG reflects light at a Bragg wavelength, and the Bragg wavelength varies with environmental changes. However, the wavelength interval of the light reflected from two FBGs with different wavelengths placed in the same environment is independent of the surrounding environment, so it can be used as a reference for the wavelength interval. Moreover, by measuring the temperatures of the FBGs and compensating for temperature-dependent changes in the reflection wavelength of the FBGs, it is possible to find the value of the reflected wavelength of the FBGs, excluding the influence of the surrounding environment with a very high accuracy.

In this paper, I propose a truly linearly tuning TLS that can achieve both a high tuning speed and a wide tuning range by utilizing a fixed etalon and one FBG as a reference device. This is accomplished by using the real-time control of a current waveform injected into a PZT-TF. By adding one more FBG, the TLS can be operated even in a linear-in-voltage mode in which the voltage across the PZT-TF increases linearly with time, so it is also possible to compare the linearity of the optical frequency change according to the operation mode of the TLS.

2. Principle and Methods

To change an optical frequency linearly with time, the gap spacing of a PZT-TF needs to be changed linearly. Therefore, if the PZT expands or contracts in proportion to the applied voltage, it is possible to implement a linearly swept TLS by driving the PZT-TF with a triangular (or sawtooth) voltage waveform. However, the PZT's elongation is not linear with the driving voltage due to non-idealities, such as non-linearity and hysteresis. It is also sensitive to changes in its surrounding environment. In order to implement a linearly swept TLS that completely eliminates the non-idealities of PZT as well as changes in PZT characteristics due to changes in its surrounding environment, it is necessary to measure changes in the optical frequency of the TLS's output and then reflect in real time the measured results in the driving waveform of the PZT via a closed-loop control. As a result, the driving voltage waveform of the PZT-TF becomes a slightly deformed triangular wave, not an exact triangular wave, and the deformation should also be changed in real time. Assuming the use of a digitally controlled linear-sweep TLS that measures the output optical frequency every τ_s and controls the magnitude of the driving signal reflecting the measured results at the corresponding section, both the principle of the TLS and the necessity of the current drive are as described below.

The triangular-voltage drive signal (only the rising part is shown in Figure 1) generated by a digital-to-analog converter (DAC) can be modeled as a series of voltage steps, as shown in Figure 1a, and for the linear tuning of a TLS, the fine control of all step heights is required, as shown in Figure 1b. The fine control of step height requires a high-bit-count and high-speed DAC. Nevertheless, due to both a voltage jump between successive steps and the dynamic transient behavior of the PZT on every voltage step [12], the linearity of the optical frequency change of the TLS cannot be guaranteed, even if it is driven with a finely controlled voltage signal, as shown in Figure 1b.

On the contrary, when a DC current is supplied to the PZT, which can be modeled as a capacitor, the voltage across the PZT becomes a ramp. While the tuning rate is actively controlled for linear tuning, the PZT current is modified into a step-added DC, as shown in

the $i(t)$ of Figure 1c. As a result, the voltage waveform becomes piecewise linear, as shown in $v_i(t)$, leading to a better linearity compared to the voltage-driven case. During a normal operation, the size of the current step is very small and the voltage waveform becomes smooth enough so no step is observed after a low pass filtering. Therefore, when it is driven by the current, the PZT voltage waveform is much smoother than that in Figure 1b, allowing for the linear tuning of the TLS. Thus, the current drive is an excellent choice as a driving method for the linear tuning of a TLS employing a PZT-TF.
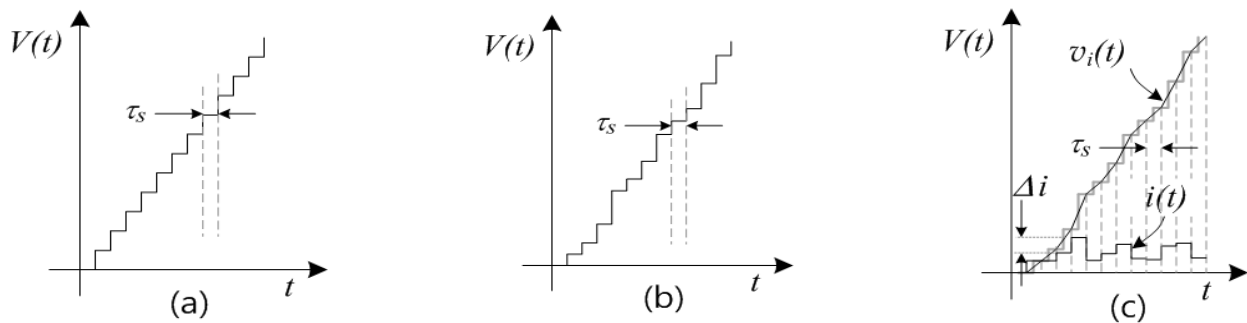

Figure 1. PZT voltage waveforms (**a**) when driven by voltage in open-loop mode, (**b**) when driven by voltage in closed-loop mode, and (**c**) when driven by current in closed-loop mode. $V(t)$ is the PZT voltage. The step height of the current ($i(t)$) is very small because the displacement of current-driven PZT is almost linear. The grey line in (**c**), which is $V(t)$ in (**b**), is added for comparison.

Now, the optical interference must be considered to figure out a sustainable way to evaluate the linearity of the linearly tuned TLS. Consider a case wherein the output from a TLS with the optical frequency $\nu(t) = \nu_o + (\gamma_o \pm \Delta\gamma)t$ (ν_o is the reference optical frequency, γ_o is the optical-frequency change rate, and $\Delta\gamma$ is the fluctuation in the optical-frequency change rate) is reflected by two mirrors (with reflectances of R_1 and R_2, respectively) separated by the distance (L). Assuming that the time needed for the light of amplitude (E_o) to travel back and forth over L is τ, the optical power (P_{out}) of the interfering light is calculated as follows:

$$\begin{aligned} P_{out} &= |E_o|^2 \left(R_1 + R_2 + 2\sqrt{R_1 R_2} \cos 2\pi[\nu(t) - \nu(t-\tau)]t\right) \\ &= |E_o|^2 \left(R_1 + R_2 + 2\sqrt{R_1 R_2} \cos 2\pi \left(\gamma_o \pm \Delta\gamma\right)\tau\, t\right) \end{aligned} \tag{1}$$

Equation (1) shows that the AC component of P_{out} is a sinusoidal wave with a center frequency of $\gamma_o\tau$ and a spectral width of $2(\Delta\gamma)\tau$. Therefore, when the output of the TLS [8] with the optical frequency $\nu(t) = \nu_o + \gamma_o t$ is fed to the interferometer, the frequency of the interferometer's output is $\gamma_o\tau$ and the spectral width of the interferometer's output is theoretically 0. However, when $\nu(t) = \nu_o + (\gamma_o \pm \Delta\gamma)t$, the interferometer's output has a bandwidth of $2\Delta\gamma\tau$ around the center frequency of $\gamma_o\tau$. Thus, $2\Delta\gamma/\gamma_o$ can be used as a measurement of non-linearity. A fiber-optic Fabry-Pérot interferometer (FFPI), consisting of two mirrors embedded inside an optical fiber, can produce a stable interference output without a polarization-induced signal fading [13]. Therefore, an FFPI can be used as a tool to measure the non-linearity in the frequency change of the TLS output. Furthermore, the spectral analysis of P_{out} can be used to find the spectral purity of the TLS output.

3. Experimental Setup and Operation

Figure 2 shows the optical system of the linearly tuned TLS driven by current. It was composed of a TF (LambdaQuest, center wavelength of 1550 nm, free spectral range (FSR) of 80 nm) [14], a polarization-insensitive semi-conductor optical amplifier (SOA, Alphion model SAC20r), and three dual-stage isolators with some directional couplers. The input of photodiode (PD) connected to two Bragg gratings (center wavelengths of 1530.22 and 1575.24 nm, respectively) was used to set the starting point and the range of the wavelength scanning.
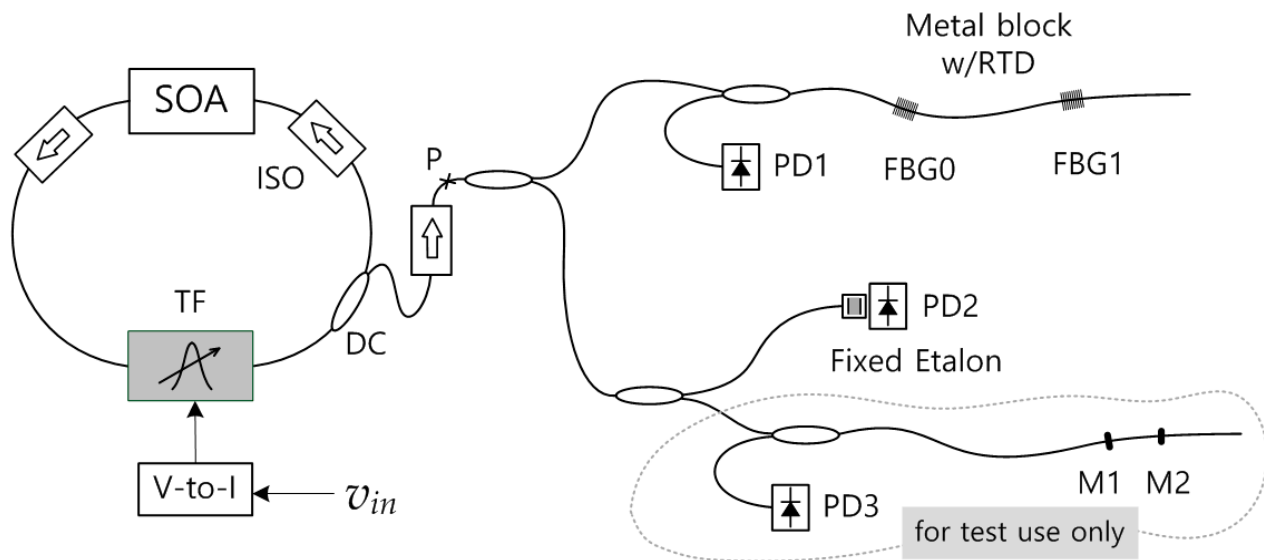
Figure 2. Optical setup: V-to-I, voltage to current converter; ISO, optical isolator (dual stage); PD, photodiode; DC, directional coupler; FBG, fiber Bragg grating; PD2, a custom-built fiber-pigtailed PD-etalon assembly; M1 and M2, mirrors inside the optical fiber.

The optical power of TLS was measured to be P = 4.7 mW, and the wavelength range of the output light was 1515 to 1595 nm. The signal processor used the outputs of two FBGs (FBG0, 1530.22 nm FBG and FBG1, 1575.24 nm FBG) that were inputs to PD1 to control both the wavelength scanning range and the scan starting point. The two FBGs were encapsulated in an aluminum block along with a resistance temperature device (RTD) so that the effect of temperature on the FBG could be accurately compensated for. A fixed etalon, which was assembled with PD2 and generated transmission peaks at 100 GHz intervals, was used to generate a reference signal to control the change rate of the optical frequency of TLS. A custom-made etalon's finesse and FSR were 20 and 100 GHz, respectively. Finally, mirrors (M1 and M2) connected to PD3 were made by embedding a dielectric mirror with a reflectivity of about 4% inside an optical fiber, and the mirrors were arranged at intervals of about 1.5 cm. The combination of these two mirrors served as an FFPI [15], so I could measure the change rate in frequency through spectral analysis of the PD3 output according to Equation (1).

Figure 3 shows a photographic image of the system configuration that combined an optical configuration and a signal-processing circuit. All the optics and electronics were mounted on 3 printed circuit boards (PCBs; for the convenience of the experiment, two of the same PD board were used). The signal processing circuit included an application-specific integrated circuit (ASIC) implemented in Intel's field-programmable gate array (FPGA; Cyclone III, EP3C25F256I7) and a PC with monitoring program. Each PCB measured 10×16 cm^2, and the electric power consumed in the whole system was ~8 W.

Consider the tuning device, PZT-TF, more closely to understand the signal-processing principle of linearly tuned TLS. The optical frequency (ν) passing through a PZT-TF with the air gap (d) is given by

$$2d\nu = pc \tag{2}$$

where p is an integer and c is the speed of light in vacuum.

When the gap is increased by Δd, the frequency change ($\Delta\nu$) of transmitted light is calculated as:
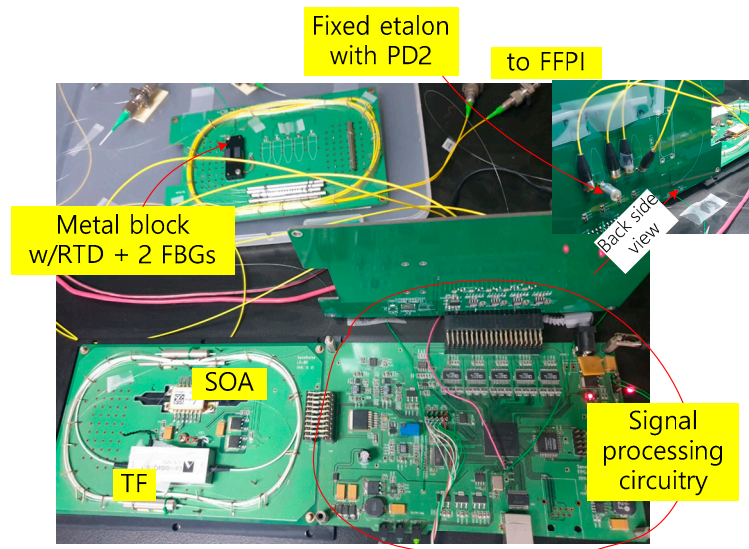
$$\Delta\nu = -(\nu/d)\,\Delta d \tag{3}$$

Figure 3. Photographic image of the experimental setup. The PD board (top right) is a picture of the backside of the PCB standing in the center.

With the help of Equations (2) and (3), Figure 4 can be used to explain the operation principle of the linearly tuned TLS. Figure 4 shows only the rising part of the sawtooth wave. When the voltage, $V(t)$, across PZT-TF increased linearly with time, the gap, $d(t)$, of TF increased linearly with slight non-linearity (hereinafter, this is expressed as "non-linearly") due to the non-linear characteristic of PZT. As a result, the frequency, $\nu(t)$, of transmitted light also changed non-linearly with time, as shown in Figure 4a. Figure 4b shows the amount of change of each variable during every τ_s period (ΔV, Δd, and $\Delta \nu$; refer to Equation (3)) when the PZT-TF voltage, $V(t)$, increased linearly with time.
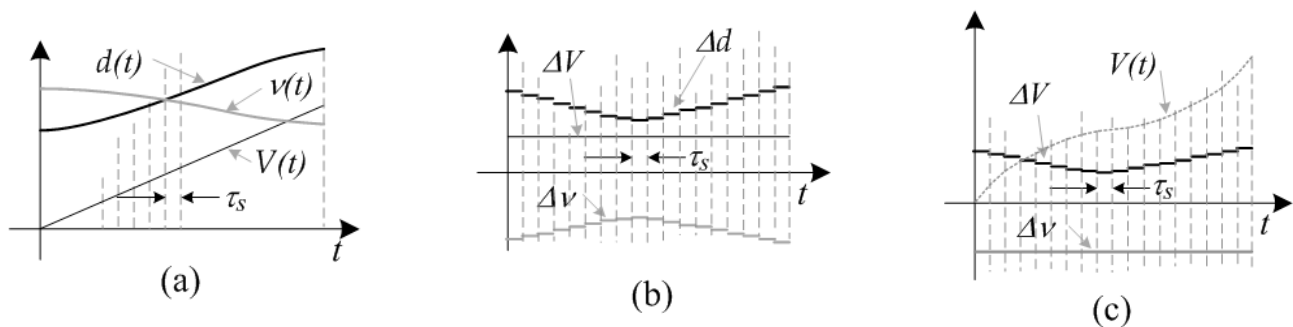

Figure 4. Operating principle of the proposed TLS: (**a**) linearly increasing PZT voltage ($V(t)$) resulting in the non-linear change in the gap ($d(t)$) and the optical frequency ($\nu(t)$) of TF, (**b**) the amount of change of each variable during τ_s when the PZT-TF voltage increased linearly with time, and (**c**) $V(t)$ showing the waveform that made $\Delta \nu$ constant.

That is, when the $V(t)$ across the PZT-TF increased linearly, the voltage change (ΔV) was constant but the optical frequency change ($\Delta \nu$) was not. Therefore, to make the $\Delta \nu$ per unit time constant, ΔV needed to be adjusted every τ_s, as shown in Figure 4c, so $V(t)$ was the waveform that made $\Delta \nu$ constant. As a result, the voltage waveform across the PZT-TF-implementing linearly tuned TLS should have been like the $V(t)$ in Figure 4c, not a straight line.

The PZT-TF in Figure 2 was driven by the V-to-I converter, for which the input was fed with v_{in} in Figure 5. Therefore, the waveform of the current flowing into TF was the same as v_{in}. As the current by V2 with a magnitude ratio of 1:7 and a duration ratio of 7:1 (sourcing:sinking) was flowing into the TF, a sawtooth voltage waveform with a slope

ratio of $(+1){:}(-7)$ (rising:falling) occurred in TF. The waveform of V2 shown in Figure 5 was generated by using a 14-bit DAC (Analog Devices, model AD9744). When the system operated in a linear-in-voltage mode, the amplitude of the sawtooth voltage generated across the PZT-TF due to the current in the V2 waveform was controlled in real time by the signal processor using the outputs of the two FBGs. For this amplitude control, a 16-bit DAC (Analog Devices, model AD5662) was used. Thus, the number of effective bits of the DAC involved in the sawtooth voltage generation was 30, and the frequency of sawtooth wave was 200 Hz.
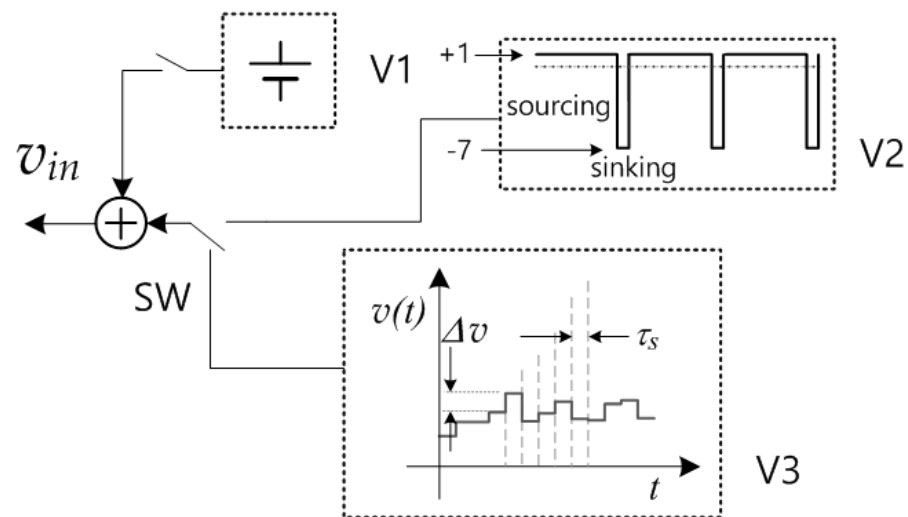

Figure 5. Input into the V-to-I converter. V1 was used to apply DC offset. V2 was the signal waveform used to generate the sawtooth waveform for PZT-TF. The ratio of sourcing to sinking was $(+1){:}(-7)$. V3 showed the signal during one sourcing period in V2. The V3 signal was the sourcing waveform of V2 plus the required deformation to keep the spacing between the transmission peaks of etalon constant. A switch, SW, was used to switch between V2 and V3 when the operating mode was changed. The deformation was updated every τ_s, which was 57.30 µs, resulting in 76 updates over every sourcing period.

The amplitude of the sawtooth voltage was controlled so that the spacing between the reflection peaks of the two FBGs was 632/854 of the sourcing period. The DC offset that needed to be added to the sawtooth voltage to locate the reflection peak of FBG0 at the 71/854 point from the start of sourcing was controlled by the magnitude and application time of V1, as shown in Figure 5, that is, by the amount of charge injected into the PZT. The signal processing unit used the reflection peaks of the two FBGs, which were fed to PD1 for the control of the amplitude of the sawtooth voltage and the DC offset. Once the control operated in the linear-in-voltage mode, the TLS maintained a scan range of 1525–1586 nm. When the operation mode was switched to a linear-in-frequency mode, the reflection peak from FBG0 was controlled to remain in the same position as in the previous mode. However, in this linear-in-frequency mode, instead of the peak spacing of the two FBGs, the transmission peak spacing of a fixed etalon input into PD2 was used to control the deformation magnitude (Δv) shown in Figure 5 to match the scan range of the previous mode. The signal processor measured each peak spacing of the fixed etalon output and used this to generate a V3 waveform in which the drive current in each segment was deformed to equalize all the peak spacings in the etalon output. Thus, two FBGs would be required to operate in the linear-in-voltage mode, whereas TLS operating in the linear-in-frequency mode would require one FBG and a fixed etalon. However, in this study, two FBGs and one fixed etalon were used to implement a TLS, which can operate in both modes of operation.

The top trace in Figure 6 shows the pulses produced by processing the PD1 output when the signal processing unit maintained the scan range of 1525–1586 nm. The bottom trace shows a V2 waveform, the period and pulse width of which were 5 ms and 4.375 ms, respectively.
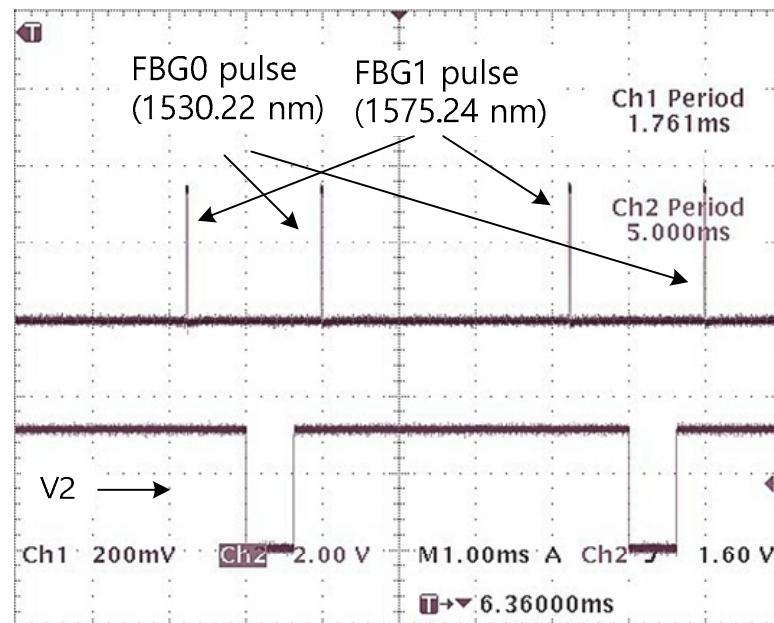

Figure 6. PD1 output pulse and V2 when the system was operating normally.

4. Results

With the scan range controlled to be 1525–1586 nm, when the operating mode was switched to the linear-in-frequency mode, V3 was used instead of V2. When the TLS operated in the linear-in-frequency mode, the output of PD2 had more than 70 gorges. Gorge-to-gorge spacing, that is, an FSR spacing of 100 GHz of the fixed etalon, was used to control the drive current of each segment in real time. There, the drive current in each segment was controlled to equalize the FSR spacing with the goal of a linearly tuned TLS. The signal-processing circuit used the transmission peak positions of the fixed etalon contained in the output of the PD2 to create the V3 by adding a deformation to the V2's waveform to keep the time interval between the etalon's transmission peaks at 57.30 μs, based on the system clock. Even in the linear-in-frequency mode, V1 continuously controlled the DC offset to keep the scanning starting point at a fixed position and V3 was the waveform with the necessary deformation added to the V2 to keep the rate of change of the optical frequency, $dv(t)/dt$, at a constant value. Since the time interval between the transmission peaks was measured based on the crystal clock of the signal-processing system, which was insensitive to changes in the surrounding environment, the frequency change rate of the TLS output was not affected by the changes in the surrounding environment.

In Figure 7, the top waveform is the measured output of the PD2 (the fixed etalon output) with an oscilloscope and the bottom trace corresponds to the V2 in Figure 5. While the V2 was zero, a current flowed out (sunk) from the PZT, and while V2 was one, a current flowed into (sourced) the PZT. Therefore, the PZT's voltage waveform was a sawtooth, falling when V2 was zero and rising when it was one. When the PZT voltage was changing from falling to rising, it was observed that the fixed etalon output for the first ~300 μs was somewhat damaged. This was caused by the bandwidth limitation of the driving circuit. Controlling the frequency change rate of the TLS based on the etalon output during this period needed to be avoided. Therefore, the frequency change rate of the TLS was controlled only after the first 300 μs within 4.375 ms of the rising time of the sawtooth waveform.
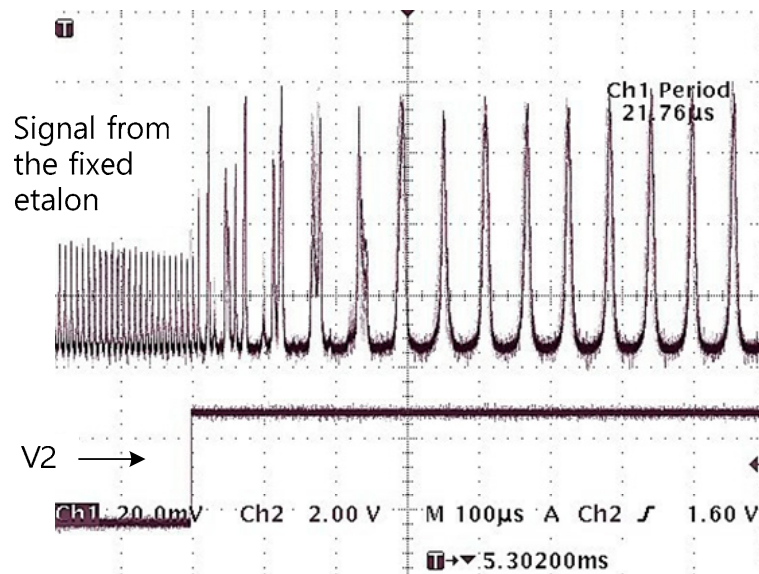
Figure 7. Output of the fixed etalon (top trace) and V2. It was observed that the waveform was not established yet for the first 300 μs.

Figure 8a shows the spectrum of PD3 output, that is, the FFPI output, when the PZT voltage increased linearly. The spectrum of PD3 output provided information on the linearity of the frequency change of the TLS output, as explained earlier. The central frequency of the spectrum was 260 kHz, and the bandwidth was measured to be about 25 kHz. Therefore, using the definition mentioned above, the degree of non-linearity was around 9.6%. Figure 8b shows the spectrum of the PD3 output when the linear-in-frequency mode was turned on to keep the change rate of the optical frequency at 1.7452×10^9 Hz/μs; it can be seen that the linearity of the frequency change of the TLS output was greatly improved. The spectral component in the frequency region lower than the spectrum peak was due to the light output during the first 300 μs of the sawtooth wave, which was excluded from the control of the driving waveform.
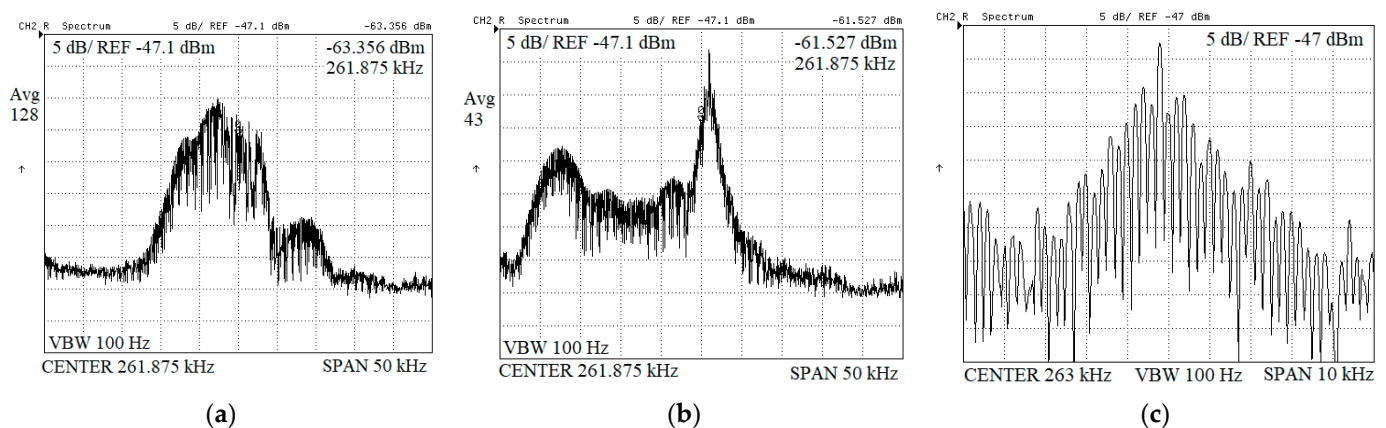

Figure 8. The spectra of PD3 outputs (5 dB/REF −47 dBm, center frequency 261 kHz) (**a**) without the waveform control (span 50 kHz) and (**b**) with the waveform control for linear tuning (span 50 kHz) and (**c**) expanded view of the spectral peak (span 10 kHz).

Figure 8c is an expanded view of the spectral peak; 200 Hz spacing sidelobes around the main peak were created because the TLS output was the amplitude modulated by the PZT drive signal. The spectral peak was located at 262.77 kHz, and the spectral width was $2(\Delta\gamma)\tau \sim 100$ Hz, which was ~1/250 of the uncontrolled case, indicating that the system was

performing its intended operation. This fairly wide spectral width of ~100 Hz suggests that the current system needs some improvement because the deformation of the V2 waveform is not accurate enough. The real-time control of the driving waveform excludes almost all the non-ideal effects of a PZT on the optical output of a TLS. The non-ideal effects of a PZT include creep and drift due to environmental changes. From the measured data, the cavity length of the FFPI used in the experiment was calculated to be 1.554 cm, assuming the refractive index (n) of the optical fiber was 1.453. Finally, I would like to point out that it is possible to use an FFPI as a reference device instead of a fixed etalon.

It is expected that the spectral intensity in the frequency region lower than the spectral peak can be significantly reduced by using a triangular wave as a driving signal and controlling the waveform during the rising period as well as the falling period. Even though the present method was demonstrated with a TLS employing a PZT-TF, the proposed method is applicable to different types of TLSs driven by both types of electrical signals—current or voltage. Furthermore, this technique is also applicable to implementations of a linear-in-wavelength or any other form TLS.

5. Conclusions

A linearly tuning TLS method with a high tuning speed and a wide tuning range in a simple configuration was proposed and experimentally demonstrated. Although this proposed method was demonstrated with a TLS employing a PZT-TF, it can be applied to all types of TLSs driven by electrical signals, whether they are current driven or voltage driven. Since the additional optical parts for linear tuning are one fixed etalon and one FBG, the use of expensive optical components is minimized. Therefore, I believe that this method could be a cost-effective solution for a linearly tuned TLS.

Conflicts of Interest: The author declares no conflict of interest. The funders had no role in the design of the study; in the collection, analyses, or interpretation of data; in the writing of the manuscript; or in the decision to publish the results.

References

1. Huber, R.; Wojtkowski, M.; Taira, K.; Fujimoto, J.G.; Hsu, K. Amplified, frequency swept lasers for frequency domain reflectometry and OCT imaging: Design and scaling principles. *Opt. Express* **2005**, *13*, 3513–3528. [CrossRef] [PubMed]
2. Nakazaki, Y.; Yamashita, S. Fast and wide tuning range wavelength-swept fiber laser based on dispersion tuning and its application to dynamic FBG sensing. *Opt. Express* **2009**, *17*, 8310–8318. [CrossRef] [PubMed]
3. Lee, H.D.; Kim, G.H.; Eom, T.J.; Jeong, M.Y.; Kim, C. Linearized Wavelength Interrogation System of Fiber Bragg Grating Strain Sensor Based on Wavelength-Swept Active Mode Locking Fiber Laser. *J. Light. Technol.* **2015**, *33*, 2617–2622. [CrossRef]
4. Soller, B.J.; Gifford, D.K.; Wolfe, M.S.; Froggatt, M.E. High resolution optical frequency domain reflectometry for characterization of components and assemblies. *Opt. Express* **2005**, *13*, 666–674. [CrossRef] [PubMed]
5. Koshikiya, Y.; Fan, X.; Ito, F. Long Range and cm-Level Spatial Resolution Measurement Using Coherent Optical Frequency Domain Reflectometry with SSB-SC Modulator and Narrow Linewidth Fiber Laser. *J. Light. Technol.* **2008**, *26*, 3287–3294. [CrossRef]
6. Yao, Z.; Mauldin, T.; Xu, Z.; Hefferman, G.; Wei, T. An Integrated OFDR System Using Combined Swept-Laser Linearization and Phase Error Compensation. *IEEE Trans. Instrum. Meas.* **2021**, *70*, 1–8. [CrossRef]
7. Badar, M.; Lu, P.; Buric, M.; Ohodnicki, P. Integrated Auxiliary Interferometer for Self-Correction of Nonlinear Tuning in Optical Frequency Domain Reflectometry. *J. Light. Technol.* **2020**, *38*, 6097–6103. [CrossRef]
8. Hsu, K. Enabling Photonics Technologies for Defense, Security, and Aerospace Applications II. 2006. Available online: https://spie.org/Publications/Proceedings/Volume/6243 (accessed on 26 March 2022).
9. Sakai, Y.; Sudo, S.; Ikegami, T. Frequency stabilization of laser diodes using $1.51-1.55$ μm absorption lines of $^{12}C_2H_2$ and $^{13}C_2H_2$. *Fiber Intgr. Opt.* **1991**, *10*, 167–181. [CrossRef]
10. Melle, S.M.; Alavie, A.T.; Karr, S.; Coroy, T.; Liu, K.; Measures, R.M. A Bragg grating-tuned fiber laser strain sensor system. *IEEE Photonics Technol. Lett.* **1993**, *5*, 263–266. [CrossRef]
11. Boucher, R.; Villeneuve, B.; Breton, M.; Tetu, M. Calibrated Fabry-Perot etalon as an absolute frequency reference for OFDM communications. *IEEE Photonics Technol. Lett.* **1992**, *4*, 801–804. [CrossRef]
12. Jung, H.; Gweon, D. Creep characteristics of piezoelectric actuators. *Rev. Sci. Instrum.* **2000**, *71*, 1896–1900. [CrossRef]

13. Vakoc, B.J.; Digonnet, M.J.F.; Kino, G.S. Demonstration of a folded Sagnac sensor array immune to polarization-induced signal fading. *Appl. Opt.* **2003**, *42*, 7132–7136. [CrossRef] [PubMed]
14. Yeh, Y.; Park, S.H. Fiber-optic tunable filter with a concave mirror. *Opt. Lett.* **2012**, *37*, 626–628. [CrossRef] [PubMed]
15. Lee, C.E.; Atkins, R.A.; Taylor, H.F. Performance of a fiber-optic temperature sensor from −200 to 1050 degrees C. *Opt. Lett.* **1988**, *13*, 1038–1040. [CrossRef] [PubMed]